Highly Organized Two- and Three-Dimensional Single-Walled Carbon Nanotube–Polymer Hybrid Architectures

Bo Li,[†,⊥] Myung Gwan Hahm,[†,⊥] Young Lae Kim,[‡] Hyun Young Jung,[†] Swastik Kar,[§] and Yung Joon Jung[†,*]

[†]Department of Mechanical and Industrial Engineering, [‡]Department of Electrical and Computer Engineering, and [§]Department of Physics, Northeastern University, Boston, Massachusetts 02115, United States. [⊥]These authors contributed equally to this work.

ABSTRACT Single-walled carbon nanotube (SWCNT) network architectures combined with flexible mediums (especially polymers) are strong candidates for functional flexible devices and composite structures requiring the combination of unique electronic, optical, and/or mechanical properties of SWCNTs and polymer materials. However, to build functional flexible devices with SWCNTs, it is required to have abilities to assemble and incorporate SWCNTs in desired locations, orientations, and dimensions on/inside polymer substrates. Here, we present unique two- and three-dimensional SWCNT network–polymer hybrid architectures by combining unprecedented control over growth, assembly, and transfer processes of SWCNTs. Several SWCNT architectures have been built on polymer materials ranging from two-dimensional suspended SWCNT microlines on PDMS microchannels to three-dimensional "PDMS-vertically aligned SWCNTs-PDMS" sandwich structures. Also a combined lateral SWCNT microline and vertically aligned SWCNT flexible device was demonstrated with good electrical conductivity and low junction resistance. The results reported here open the pathway for the development of SWCNT-based functional systems in various flexible device applications.

KEYWORDS: hybrid architectures · flexible · transfer · single-walled carbon nanotube

Over the past decade, artificially engineered carbon nanotube architectures, designed for a range of micro- and macroscopic functional devices, have made remarkable progress.[1−9] To a large extent, these architectures also represent a significant advance in the fabrication of either randomly arranged or aligned nanotubes (horizontal or vertical) stamped on, or embedded within, a chosen polymer or similar matrix, which finds applications in flexible electronic,[4,5] optoelectronic,[1] and field emission devices.[7] However, despite these progresses, the fabrication of scalable and tightly controlled multidimensional microscale functional flexible systems that harness horizontal as well as vertical architectures of organized single-walled carbon nanotubes (SWCNTs) has remained largely elusive. Such methodologies would allow a seamless integration of SWCNT-based functional elements (*e.g.*, field emission pixels[7] and active sensing arrays[10]) with the possible flexible SWCNT-based circuitry constructed in a flexible matrix, enabling highly functional all-SWCNT flexible devices. Developing and fine-tuning methods that not only maintain multidimensional structural integrity but also high-quality electrical properties (especially at junctions and interfaces) of the said hybrid structure has so far remained a considerable practical challenge. Further, maintaining scalability of such a process up to macroscopic dimensions that would enable realistic devices is an additional roadblock.

Here, we present a new class of highly organized SWCNT network–polymer hybrid structures, by incorporating horizontally and vertically aligned SWCNTs in desired locations, orientations, and dimensions on/inside flexible polymer matrices forming mechanically and electrically robust unique two- and three-dimensional architectures previously undemonstrated. Several architectures have been built ranging from two-dimensional suspended SWCNT microlines on microtrenched PDMS substrates to three-dimensional "PDMS-vertically aligned SWCNTs-PDMS" sandwich structures. Finally, a combined structure comprising lateral SWCNT microlines and vertical SWCNTs embedded in a flexible matrix is also demonstrated, highlighting the scalability and robustness of the fabrication process. These hybrid structures which combine horizontal and vertical structures of SWCNTs were found to have reasonably good electrical properties, especially low junction resistances, representing an unprecedented control over growth, assembly, and transfer

* Address correspondence to jungy@coe.neu.edu.

Received for review March 6, 2011 and accepted May 24, 2011.

Published online May 24, 2011
10.1021/nn2008782

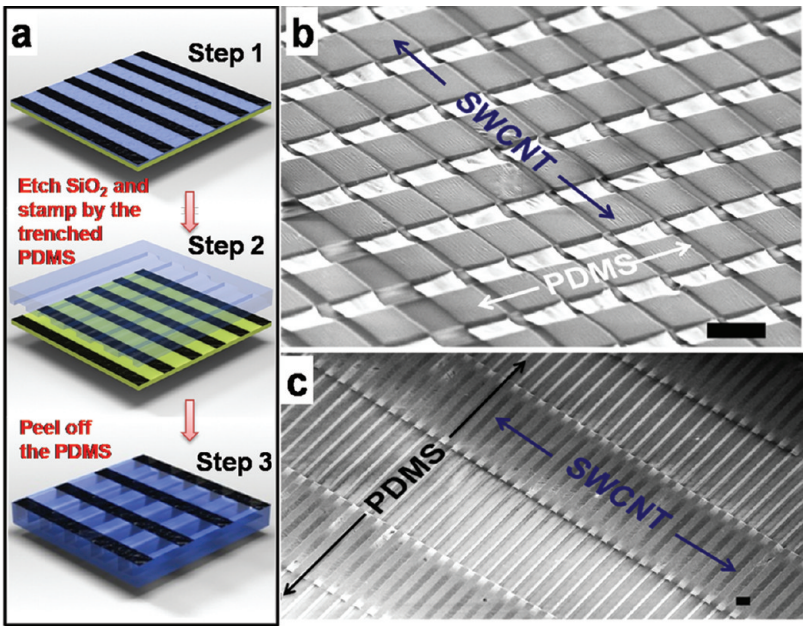

Figure 1. Suspended SWCNT−polymer hybrid structures: (a) schematic of wet-contact stamping method. Step 1: SWCNTs were assembled into aligned microline structures (black lines) on a Si substrate (yellow layer) with a SiO_2 sacrificial layer on the top (blue layer). Step 2: SiO_2 was etched using diluted HF acid solution, and then a PDMS stamp (blue and transparent) patterned with microtrenches on the bottom was brought in contact with the SWCNT/Si substrate at a right angle with respect to the arrays of SWCNT microlines. Step 3: PDMS stamp inked with suspended SWCNT microlines was peeled off, put upside down, and dried in ambient conditions. (b) Highly ordered arrays of 1 cm long SWCNT microlines (9 μm in width) suspended across PDMS microtrenches (6 μm in width, 3 μm in depth, and the distance between nearby trenches is 9 μm). (c) Larger SWCNT microlines (100 μm in width) suspended on similar PDMS microtrenches but at larger depth (6 μm). Scale bars are 10 μm for panels b and c.

processes of SWCNTs into unique two- and three-dimensional network architectures.

In order to build the integrated SWCNT-based flexible systems, it is required to place highly organized and aligned SWCNT network architectures inside or on flexible polymer substrates with controlled orientations, geometries, and dimensions. To achieve this, three methods have been developed and employed: controlled growth,[11−13] a well-defined fluidic assembly,[14−17] and a precise transferring of SWCNTs.[3,5,18] To create complex two- and three-dimensional SWCNT-based flexible systems, a combination of both or all three of these techniques was required. We first designed and built horizontally and vertically organized SWCNT network architectures at the microscale on SiO_2/Si substrates using a template-guided fluidic assembly and chemical vapor deposition (CVD) methods, respectively. For horizontally organized SWCNT network structures, a plasma treatment was used to enhance the hydrophilic nature of SiO_2 surfaces. Then, a photoresist film, hydrophobic to a SWCNT solution, was lithographically patterned to assemble SWCNTs into predesigned network structures following the hydrophilic SiO_2 surface patterns. To create millimeter scale long, organized, and vertically aligned SWCNT structures, a highly effective ethanol CVD was conducted on micropatterned Co catalyst films. The preference of SWCNTs to grow normal to, and selectively on, catalyst-deposited surfaces forced the SWCNTs to inherit the topography of the patterned Co catalyst film, resulting in vertically aligned and organized SWCNT microarchitectures of well-defined geometries. Then, these two- and three-dimensional SWCNT microarchitectures were transferred onto the surface or inside selected polymer matrices using wet-contact stamping, cast-etching, and polymer casting transfer methods without disturbing the alignment, shape, and dimension of the original SWCNT network architectures.

RESULTS AND DISCUSSION

Figure 1 shows striking examples of organized SWCNT microlines suspended on polydimethylsiloxane (PDMS) microtrenches. Our approach for fabricating these unique structures is shown schematically in Figure 1a. First, arrays of SWCNT microlines (black strips, step 1) were created on the SiO_2 (shown in blue) substrate by using the above-mentioned fluidic assembly of SWCNTs. Then the substrate was dipped into a diluted HF acid solution to remove a SiO_2 sacrificial layer and taken out without drying the surface, followed by an immediate stamping with a prepatterned PDMS substrate (illustrated as the transparent blue substrate, step 2). This wet-etching process greatly attenuates the adhesion between SWCNT patterns and the underlying substrate, and when the PDMS stamp is peeled off (step 3), it allows an extremely effective transfer of the horizontally aligned SWCNT microlines onto the patterned PDMS surface. Figure 1b

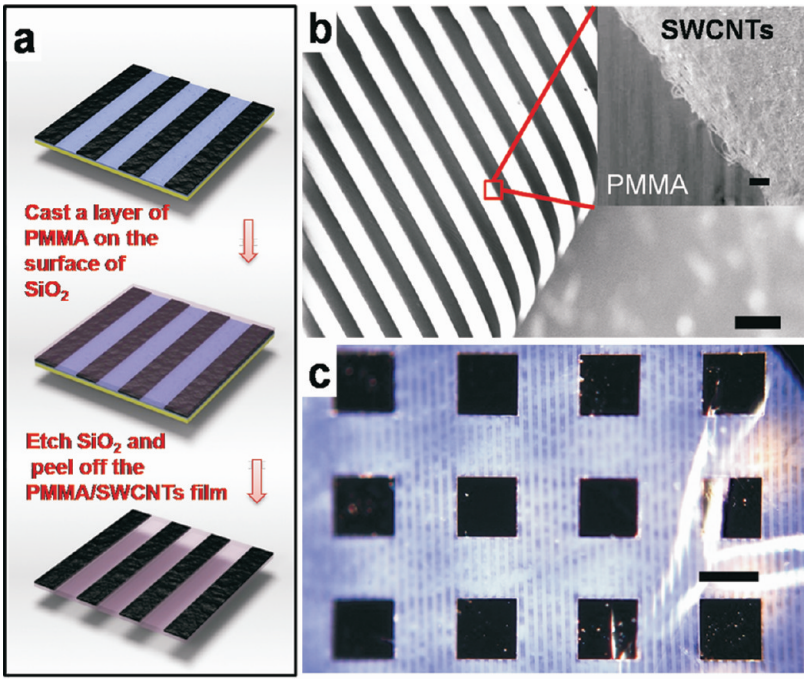

Figure 2. Embedded SWCNT–polymer hybrid structures: (a) schematic of cast-etching method. The polymer (PMMA, pink layer) was casted onto the SWCNT/SiO_2/Si substrate, followed by etching the SiO_2 layer and peeling off the SWCNTs/PMMA film. The final image shows the top view after the SWCNTs/PMMA was turned upside down. (b) SEM image of a folded region of flexible SWCNTs/PMMA film. Inset image shows the boundary between SWCNTs and PMMA. (c) Optical image of SWCNT microlines transferred on the thin PMMA film together with gold contact pads (100 μm $\times$ 100 μm, 150 nm thick). The gold pad was patterned on SiO_2/Si substrate before the assembly of SWCNTs. Therefore, after transferred film was turned upside down, Au microcontact pads (squares) are placed on the top of SWCNT–PMMA film. Scale bars are (b) 20 μm (scale bar of inserted SEM image is 200 nm) and (c) 100 μm.

shows arrays of centimeters long and aligned SWCNT microlines (9 μm in width and 10–20 nm in thickness) suspended orthogonally across PDMS microtrenches (6 μm in width, 3 μm in depth, and 9 μm in space between the nearby trenches). Note that the self-adhesion between the nanotubes is robust, and hence it allows a perfect transfer even in the trench regions, where the mechanical support of PDMS is absent. To our knowledge, such highly organized, suspended, and ultrathin microscale architectures of SWCNTs on three-dimensionally patterned, flexible substrates have never been demonstrated before. These suspended SWCNT microlines are potentially useful for highly sensitive sensing applications within microfluidic channels, mechanical sensing, optical sensing, and chemical/gas sensing *etc*. As shown in Figure 1c, this method can be applied to fabricate larger SWCNT patterns where the SWCNT microlines (100 μm in width) were transferred across the PDMS microtrenches with a larger depth (6 μm). These horizontally aligned SWCNT microlines could also be transferred into other polymer films such as poly(methyl methacrylate) (PMMA), as shown schematically in Figure 2a. For this, a layer of PMMA was casted on SWCNT microlines and cured such that the SWCNTs were held by the PMMA polymer. Then, the PMMA polymer layer with SWCNT microstructures could be peeled off from the donor substrate by etching the SiO_2 sacrificial layer in a diluted HF acid solution. The mechanical flexibility of such structures can be seen in Figure 2b, which shows the curved end of SWCNT microline–PMMA film, and the inset figure clearly indicates the well-defined boundary between assembled SWCNT microlines and the PMMA substrate. Along with SWCNT microlines, we were also able to simultaneously transfer gold microcontacts, deposited on the initial SiO_2 surface before the assembly of SWCNTs forming the flexible device ready for electrical measurement. (Note that our developed SWCNT fluidic assembly method can be applied not only to silicon-based substrates but also to other metal surfaces.) Figure 2c shows an optical micrograph of these structures, where the dark squares represent the Au contacts formed on SWCNT microlines and PMMA film.

This nanotube transfer strategy could be extended to fabricate diversely designed vertically aligned SWCNT–flexible polymer hybrid structures. For example, vertically aligned SWCNTs grown on the SiO_2/Si substrate can be partially planted on the surface of flexible polymer substrates through a controlled contact polymer casting transfer process and subsequent peeling off from the original SiO_2 substrate. A schematic representing this process is shown in Figure 3a. For this, arrays of vertically aligned SWCNTs (depicted in black columns in schematics) were grown on the SiO_2/Si substrate using an ethanol CVD

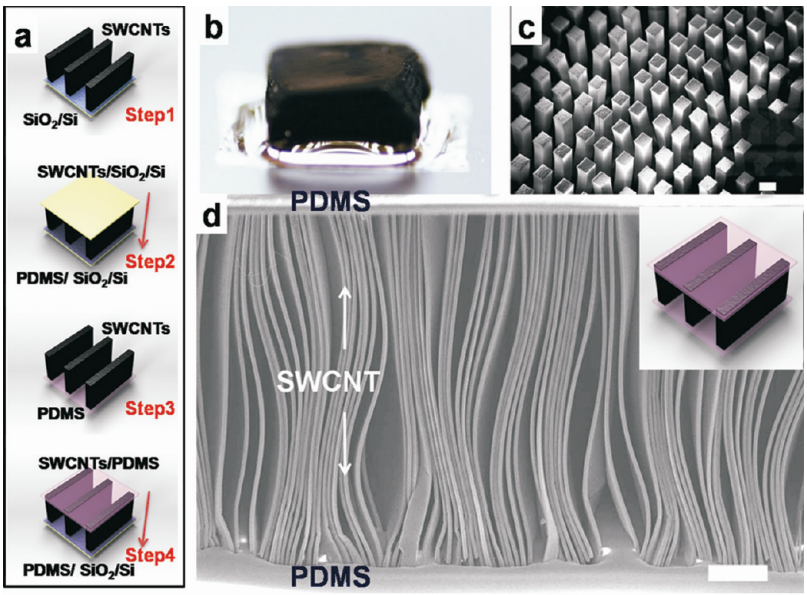

Figure 3. Vertically aligned and organized three-dimensional SWCNT−polymer hybrid structures. (a) Schematic of contact polymer casting transfer method. Step 1: vertically aligned SWCNTs were grown on a SiO_2/Si substrate with prescribed shape. Step 2: SWCNTs/SiO_2/Si substrate is turned upside down and brought in contact with a second SiO_2/Si substrate cast with PDMS. The top layer of PDMS is not cured and can hold the SWCNTs during the following curing process. Step 3: after the PDMS was completely cured, the SiO_2/Si substrate on both sizes can be detached mechanically, leaving SWCNTs planted on PDMS. Step 4: SWCNTs/PDMS can be turned over and brought in contact with another PDMS/SiO_2/Si substrate, forming a sandwiched PDMS/SWCNTs/PDMS structure. (b) Optical image of vertically aligned 3 mm long SWCNT film planted on the top surface of the thin PDMS film (300 μm thick). (c) Square patterned vertically aligned SWNCT micropillars (100 μm × 100 μm) planted on the thin PDMS film. (d) Cross-sectional SEM image shows vertically aligned SWCNT microlines (9 μm in width and 6 μm in space) placed between two thin PDMS films resulting in a PDMS/SWCNTs/PDMS sandwich structure. Scale bars are 100 μm.

method (step 1). Then, this SWCNTs/SiO_2/Si substrate was turned upside down and brought in contact with a very thin layer of uncured PDMS spin-coated on the SiO_2/Si substrate (step 2). After the PDMS was completely cured, the SiO_2/Si substrate on both sides can be detached leaving free-standing SWCNTs directly planted on the surface of PDMS films (step 3). Figure 3b,c shows optical and SEM images of vertically aligned few millimeters long SWCNT arrays and micropillar structures planted on the top surface of the thin PDMS film, respectively. The length of SWCNTs planted into the surface of PDMS could be controlled by changing the thickness of uncured PDMS film to obtain an effective transfer of vertically aligned SWCNTs with the desired exposed length of SWCNTs. By using the two-step contact polymer casting transfer method described above, we could also place vertically aligned and millimeters long SWCNT arrays or micropatterns between two PDMS films, thereby forming unique PDMS/vertically aligned SWCNTs/PDMS sandwich structures (step 4 in Figure 3a,d). The inset schematic of Figure 3d indicates the three-dimensional perspective view of the PDMS/vertically aligned SWCNTs/PDMS sandwich structure that we fabricated. It should be noted that the good wettability of PDMS on SWCNTs enables the casted thin PDMS films to anchor the top and bottom of vertically aligned SWCNT structures, effectively providing mechanically strong interfaces between SWCNTs and PDMS substrates.[19] These macroscopic but nanostructured confined hybrid systems having extremely high active specific surface area of SWCNTs provides unique opportunities for developing multifunctional membrane devices such as molecular or ionic exchangers,[20] high-surface thermal exchangers,[21] chemical/gas sensors,[10] and gas storage technologies within flexible environments.[22]

Further, we explored the potential for combining lateral and vertical SWCNT structures to construct three-dimensionally ordered electrically conducting networks inside of polymer materials. Figure 4 shows schematics and micrographs of vertically aligned SWCNT line patterns impregnated into a thick transparent PDMS matrix and interconnected with horizontally aligned SWCNT microlines and gold contact pads placed on the top and bottom of the PDMS substrate. To fabricate such an architecture, first, three columns of vertically aligned SWCNT line structures (Figure 4a,b) were inserted inside a bulk PDMS matrix by casting a thick layer of PDMS covering the length of vertically aligned SWCNTs and then curing it.[7] Then, the top and bottom surfaces of a PDMS substrate were mechanically polished to expose both ends of vertically aligned SWCNTs. Each side of this polished PDMS/vertically aligned SWCNT substrate was used as a stamp to transfer a layer of optically transparent ultrathin horizontal SWCNT microlines (9 μm width) together with

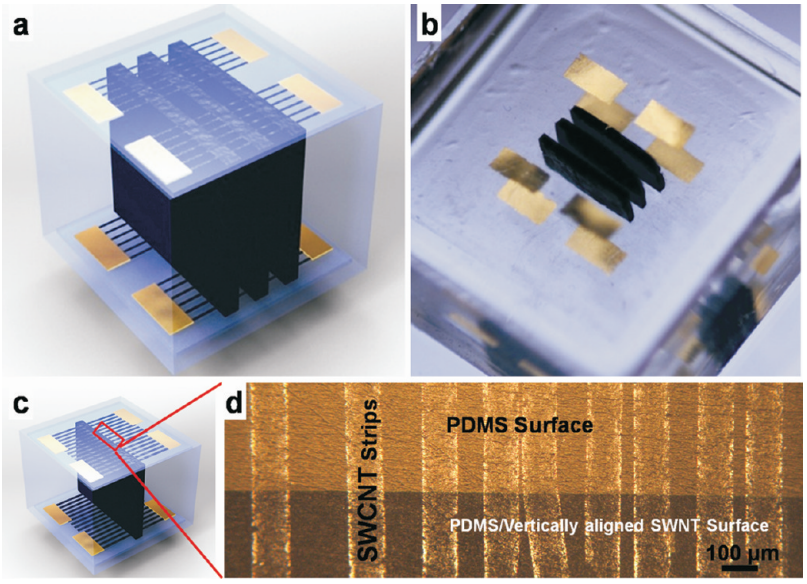

Figure 4. Combined lateral SWCNT microlines and vertically aligned SWCNT arrays inside PDMS substrates. (a) Schematic of combined three-dimensional lateral SWCNT microlines and vertical SWCNT−polymer hybrid structures. (b) Optical image showing horizontal and vertical SWCNT networks along with gold contact pads inside a centimeter thick PDMS matrix. Note that vertically aligned SWCNT line structures (3 mm height, 7 mm length, and 700 μm width) are shown in black inside a transparent PDMS substrate and physically contacted by arrays of SWCNT microlines (9 μm in width and 6 μm in space, transparent in the optical image) with a 90° angle on the top and bottom of a PDMS substrate. (c) Schematic of combined three-dimensional SWCNT−polymer hybrid structures for electrical measurement with only one column of vertically aligned SWCNTs and 100 μm wide SWCNT microlines. (d) Optical microscopy image of centimeters long and 100 μm wide SWCNT microlines interconnected to the vertically aligned SWCNT structure inside the PDMS matrix. Pure PDMS regions are shown in a bright contrast, while the PDMS-vertically aligned SWCNT composite structures are shown in a dark contrast.

gold contact pads on each end, using the wet-contact stamping method as shown in Figure 1a.

Finally, the whole sample was sealed in the PDMS. We show that despite the mechanical polishing applied to the vertically aligned SWNTs, their mechanical interface with the horizontal SWCNT architectures showed surprisingly low contact resistance. This is indeed very encouraging since no extra process steps were undertaken to improve the physical proximity of the vertical and horizontal nanotubes, other than the mechanical contact obtained directly through the transfer process. For electrical measurement, we used a simpler structure with only one column of vertically aligned SWCNTs and 100 μm wide SWCNT microlines, as illustrated in Figure 4c. Figure 4d is the optical microscopy image showing continuous and aligned 100 μm wide SWCNT microlines lying across the boundary between pure PDMS and PDMS-vertically aligned SWCNT composite regions.

The current−voltage (I−V) measurements conducted between the contact pad A and all other contact pads are plotted in Figure 5a, showing a linear dependence of current with voltage, indicating that well-defined conductive paths are built from the contact pad A to other contact pads, and Ohmic interfaces have been established at every single SWCNT junction. The linear fit of I−V is provided in Supporting Information. The labeling of the contact pads is shown in the inset. The values of electrical resistances between any two existing contacts are summarized in the Table 1. Note that for all measured pairs of contact pads, the conducting paths are a combination of lateral SWCNT microlines and vertically aligned SWCNTs, except the conduction path along the same lateral SWNT microlines (*e.g.*, between the contact pads A and B). The average electrical resistance measured between contact pads that included both horizontal and vertical architectures was found to be 14.16 kΩ. The average electrical resistance only for the lateral SWCNT structures within the same plane was 13.03 kΩ. This indicates that the total resistance was largely dominated by the ultrathin lateral nanotube lines, which is not surprising because the vertical columns have much larger cross sections. Since the vertically aligned SWCNT structure was interconnected with the lateral SWCNT microlines, the resistance in the combined three-dimensional networks is higher than that of the horizontally assembled SWCNT structures. In addition, uniformly distributed electrical resistances within the three-dimensional SWCNT network indicate that contacts between lateral SWCNT microlines and vertically aligned SWCNTs are quite stable for most of the macroscopic conduction paths.

The resistance values obtained between pairs of contact pads A−a, A−B, a−b, and B−b could be used to estimate the upper limit of the junction resistance between horizontal SWCNT microlines and vertically aligned SWCNTs for a given three-dimensional structure.

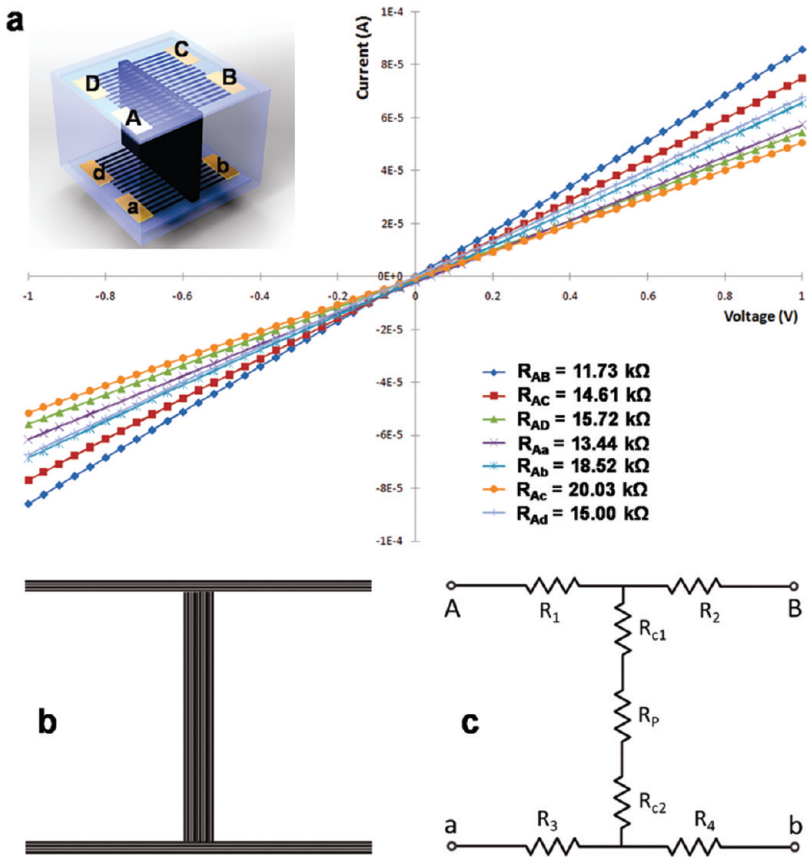

Figure 5. *I*−*V* measurement of the combined three-dimensional SWCNT device. (a) Line graph shows the measurement from contact pad *A* to all the other contact pads in a macroscopic SWCNT network inside the PDMS substrate. (b) Cross-sectional schematic of three-dimensional horizontal and vertical SWCNT network and (c) its circuit model indicating a device resistance and contact resistance between the horizontally aligned SWCNTs and vertically aligned SWCNTs.

TABLE 1. Resistance between All the Existing Pairs of Contact Pads Calculated from the *I*−*V* Measurement

Resistance (kΩ)	A	B	C	D	a	b	c	d
A		11.73	14.61	15.72	13.44	18.52	20.03	15.00
B			10.89	10.19	8.08	11.99	13.79	9.00
C				13.10	17.51	16.84	18.61	13.70
D					10.84	16.02	17.74	12.71
a						13.21	15.51	10.50
b							18.45	14.70
c								14.09
d								

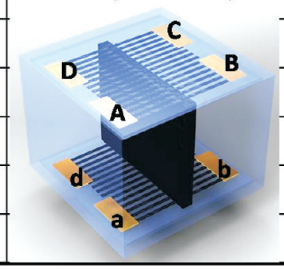

Figure 5b shows the cross-sectional schematic of three-dimensional SWCNT networks, and Figure 5c shows its circuit model consisting of nanotube resistances and the junction resistance between horizontal and vertical SWCNT networks. The measured resistance between the contact pads *A* and *a* can be written as $R_{Aa} = R_1 + R_{c1} + R_P + R_{c2} + R_3$, where R_{c1} (or R_{c2}) = nanotube−nanotube contact junction resistance between horizontal and vertical SWCNTs and R_P = device resistance of the intermediate pillar structure. In this way, the junction + pillar resistance of a three-dimensional architecture can be estimated using the

following equation: $R_{Aa} + R_{Bb} = R_{AB} + 2(R_{c1} + R_P + R_{c2}) + R_{ab}$. Using the measured values of the other quantities, $R_{c1} + R_P + R_{c2}$ in the parentheses was found to be 0.5375 ± 0.2925 kΩ. The detailed calculation of contact resistance as well as the resistance of SWCNT leads (R_1 to R_4) can be found in the Supporting Information. Since the resistance of the pillar is additive to the junction resistance, it was not possible to eliminate its value, and hence the quantity $R_{c1} + R_P + R_{c2}$ represents the absolute upper limit to the the junction resistance. In reality, the junction resistance was even smaller since we know that the pillar resistance is never = 0 Ω. With the measured resistance of R_{Aa} or R_{Bb}, we calculate the percentage of pillar + junction resistance by dividing $R_{c1} + R_P + R_{c2}$ and found that the percentage of contact resistance is 4.0 or 4.5%, respectively. On the other side of the structure, the percentage of contact resistance is 11.2 or 16.5% depending on the measured resistance for R_{Cc} or R_{Dd}. Even though we assume that contact resistances are much higher than the resistance of a pillar structure, horizontal and vertical SWCNT junction contact resistances are within 3.0 to 16.5% of the total resistance in this three-dimensional network, showing stable and low electrical contacts between horizontal and vertical SWCNT structures.

The mechanically and electrically robust SWCNT-PDMS array structures form an ideal platform for the development of flexible microfluidic lab-on-chip architectures.[23−26] In such architectures, fluids are allowed to mix in small quantities in a controlled way and often require embedded electronics for heating, detection, and electrochemistry in optically transparent micrometer size arrays of well-designed channels. To demonstrate a *proof-of-principle* microchannel sensor using our hybrid structures, we designed a SWCNT-PDMS channel architecture as shown in Figure 6a, which consists of parallel arrays of aligned and suspended SWCNT two-dimensional microlines placed orthogonally across arrays of micrometer scale PDMS trenches. The PDMS cell with trenches at the bottom was fabricated by casting uncured PDMS onto a SiO_2/Si substrate patterned with SU-8 strips (7.5 μm in width and 7.5 μm in space between the strips and 6 μm in height). After being cured, the PDMS cell was peeled off from the substrate, leaving trenches with reciprocal size on the bottom. A set of four 100 μm wide SWCNT microarrays was then transferred to the trenched region of the PDMS cell by the method of wet-contact stamping followed by depositing Ti/Au (5 nm/150 nm) contact pads at the end of SWCNT microline structures, leaving a 1.5 mm gap between the two contact pads. Since it is difficult to image the SWCNTs on PDMS due to the charging and deformation of PDMS under electron beam, the SEM images were taken from the SWCNT region coated with Ti/Au. As shown in Figure 6b, the arrays of SWCNT microlines sit at a right angle with respect to the PDMS trenches, and a higher magnification

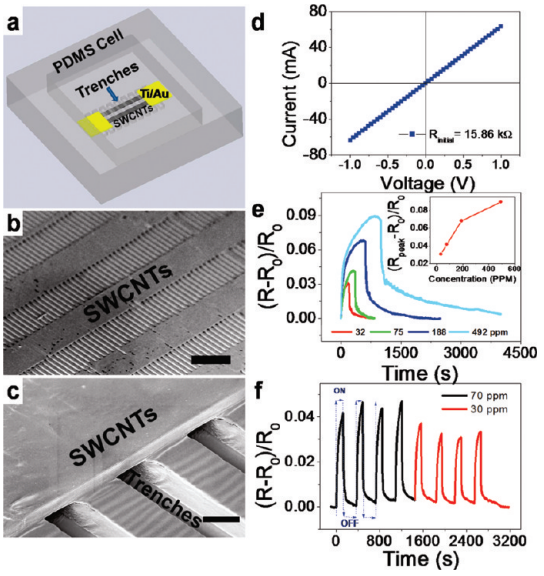

Figure 6. Ethanol sensor based on suspended SWCNTs. (a) Schematic of suspended SWCNT ethanol gas sensor. (b) SEM image of the suspended SWCNT gas sensor. (c) SEM image of the edge of suspended SWCNT microlines. (d) *I*−*V* curve of gas sensor before the gas sensing experiment. (e) Electrical response of suspended SWCNT microlines with respect to four different concentrations of ethanol. The SWCNTs were exposed to ethanol until the resistance reached the peak value followed by releasing the ethanol in atmosphere. The resistance difference ($R-R_0$) was normalized with respect to the initial value (R_0) of each run. (f) Test of reproducibility for two different concentrations (70 and 30 ppm). Scale bars are 100 μm for panel b and 5 μm for panel c.

image in Figure 6c clarifies that the SWCNTs are suspended across the trenches of PDMS. Although, in principle, the SWCNT network structures could be independently attached to electrical contact pads, but for the ease of demonstration, they were electrically shorted at each end as shown using Ti/Au contact pads. Previous work has shown that interaction with ethanol molecules can change the electrical properties of SWCNTs, leading to fast response and good reversibility.[27] We utilize this fact to test our highly organized, flexible, and suspend SWCNT microarchitecture as an ethanol sensor using varying concentrations of ethanol vapor.

The initial resistance of our sensor was 15.86 kΩ, as shown in Figure 6d, and the linear *I*−*V* curve indicates good Ohmic contact between SWCNTs and contact pads. The electrical response as a function of ethanol concentration as well as the reproducibility is shown in Figure 6e,f, respectively. In Figure 6e, the electrical response to four different concentrations, ranging from 30 to 500 ppm, are presented. The sensitivity ($(R_{peak}-R_0)/R_0$) of the sensor (inset in Figure 6e) increases from 3 to 9% with the increase of concentration from 30 to 500 ppm. The electrical response in Figure 6e shows good reproducibility for four continuous cycles under two different concentrations. The on and off times were set to be 120 and 240 s. The results

feature a rapid response and almost complete recovery of the suspended SWCNT sensors, indicating that there were no chemical bonds between the ethanol molecules and the sensing surface since such bond formation is usually associated with large time scales and no recovery. It has been shown that the absorption efficiency of the polar organic molecules with hydroxyl groups in substances involving carboxyl molecules increases due to electrostatic dipole−dipole interactions.[28] The SWCNT microlines were fabricated from SWCNT−DI water solution by the method of guided fluidic assembly.[29] To achieve good dispersion of SWCNTs in DI water, the surface of SWCNTs was functionalized with −COOH groups. From this fact, the main sensing mechanism in our sensor system appears to be hydrogen bonding between a hydrogen atom with a positive partial charge on the −OH group of the ethanol and a negatively charged oxygen atom within the −COOH functional groups on the SWCNTs. Therefore, the increase in resistance we have observed in all measurements is most likely due to hydrogen bond formation.

To summarize, we have presented mechanically and electrically robust novel two- and three-dimensionally organized and aligned SWCNT network−polymer hybrid structures. Our fabrication method is scalable and uses CMOS compatible methods and hence is extremely valuable for integration with the current microfabrication technology. Further, the potential application of suspended SWCNTs was demonstrated by constructing a gas sensor with good sensitivity and reproducibility to ethanol. These multidimensional microscale SWCNT network−polymer hybrid structures have immediate and immense implications for the development microscale multifunctional flexible systems such as sensors, actuators, interconnects, transparent flexible electrodes, advanced microfluidic devices, and smart membrane systems.

EXPERIMENTAL SECTION

Assembly of Two-Dimensional SWCNT Microlines. SiO_2/Si chip was used as a substrate for the template-guided fluidic assembly of SWCNTs. The SiO_2 layer acts as an assembly surface for SWCNTs and sacrificial layer in the following SWCNT transfer process. The SWCNT/deionized (DI) water solution (0.23 wt %) was obtained from Brewer Science Corp, USA. In order to improve the contact between the SWCNT/DI water solution and substrate, the SiO_2 surface was pretreated with the mixture of SF_6 (20 sccm), O_2 (20 sccm), and Ar (5 sccm) plasma for 5 s.[29] After that, a photoresist film was spin-coated and patterned into desired microline structures using an optical lithography process. The patterned substrate was then vertically submerged into the SWCNT/DI water solution and gradually lifted up from the solution with a constant pulling speed, 0.1 mm/min for 9 μm wide microlines and 0.05 mm/min for the 100 μm wide microline structures.[16,29]

Millimeter Scale Long Vertically Aligned SWCNT Growth. Vertically aligned SWCNTs were grown on Co/Al/SiO_2 multilayered substrate using an ethanol chemical vapor deposition (CVD) method.[30] First, a 20 nm thick Al layer was deposited onto a SiO_2 wafer as a buffer layer to grow vertically aligned SWCNTs. On the top of the Al/SiO_2 layer, a 0.7−1 nm thick Co catalyst film was deposited using an e-beam evaporator. The Co/Al/SiO_2 multilayered substrate was then annealed at 850 °C for 10 min to form uniform catalyst nanoparticles with 5% hydrogen balanced argon mixture gas.[31] To grow vertically aligned SWCNTs, ethanol vapor was supplied as a carbon source for 1 h with 50 sccm flow rate at 850 °C. To create vertically aligned and organized SWCNT microstructures, a Co catalyst thin film was patterned on Al/SiO_2 substrate using a conventional optical lithography process.

Contact Polymer Casting Transfer Method. To transfer vertically aligned SWCNTs on the surface of PDMS substrates, a thin PDMS film (300 μm) was spin-coated on SiO_2/Si chip (1 cm × 1 cm). The ratio of precursor and curing agent was 10:1, and the film was cured for 30 s at 110 °C on a hot plate. As-grown vertically aligned SWCNTs were then attached to the thin PDMS film and cured for another 1 min at 110 °C. Since the interface between SWCNTs and SiO_2/Si is very weak, SWCNTs could be easily detached from the original substrate with the other end strongly held by the thin PDMS film. To fabricate the PDMS/SWCNTs/PDMS sandwich structure, a two-step PDMS casting transfer method was conducted. After the first transfer process, the original roots of SWCNT patterns become free ends, and it can be transferred to another thin PDMS film following the same procedure as the first time transfer.

Fabrication of the Combined Three-Dimensional SWCNT/Polymer Architecture. To construct the combined three-dimensional SWCNT architecture inside a thick PDMS matrix, a combination of wet-contact stamping method and polymer casting transfer method was applied. First, vertically aligned SWCNT line structures were inserted in a bulk PDMS substrate using a polymer casting transfer method by casting a thick layer of PDMS covering the length of vertically aligned SWCNTs and then cured. After that, the top and bottom surfaces of a PDMS substrate were mechanically polished using sandpaper with small grit size (P3000) to expose both ends of vertically aligned SWCNTs and maintain low surface roughness. The PDMS/vertically aligned SWCNT substrate was used as stamp and orthogonally contacted by two layers of optically transparent two-dimensional SWCNT microlines together with gold contact pads after the SiO_2 underneath was removed by using a diluted HF acid solution. The transferred sample was further rinsed in DI water for 10 min to remove the chemical residue. For electrical measurement, copper wires were attached to the gold contact pads using silver paint. The whole device was then sealed in PDMS.

Ethanol Sensing. The ethanol sensing experiment is processed in a well-sealed chamber, and the electrical data are real-time collected using Agilent 4156C. For the measurement of electrical response as the function of ethanol concentration, the ethanol vapor was infused into the chamber which was kept closed until the resistance reached the peak value. Then the chamber was opened to the atmosphere to release the ethanol. Four different concentrations (32, 75, 188, and 492 ppm) were tested in our experiment. The sensitivity $((R_{peak}-R_0)/R_0)$ was calculated by normalizing the difference between peak resistance and the initial resistance R_0. For the test of reproducibility, two concentrations have been selected (70 and 30 ppm) and four continuous running cycles were processed for each concentration. For each cycle, the exposing time (on status in Figure 6f) and the recovery time (off status in Figure 6f) were set to be 120 and 240 s, respectively.

Acknowledgment. The authors acknowledge the financial support from Fundamental R&D Program for Core Technology of Materials in the Ministry of Knowledge Economy, Republic of Korea, National Science Foundation-CMMI grant (0927088), and

Center for High-Rate Nanomanufacturing in Northeastern University. S.K. acknowledges partial support by NSF ECCS 1102481. Work was performed in the George J. Kostas Nanoscale Technology and Manufacturing Research Center at Northeastern University.

Supporting Information Available: Additional calculation details of combined three-dimensional SWCNT–polymer hybrid architecture. This material is available free of charge *via* the Internet at http://pubs.acs.org.

REFERENCES AND NOTES

1. Wu, Z.; Chen, Z.; Du, X.; Logan, J.; Sippel, J.; Nikolou, M.; Kamaras, K.; Reynolds, J.; Tanner, D.; Hebard, A. Transparent, Conductive Carbon Nanotube Films. *Science* **2004**, *305*, 1273–1276.
2. Hinds, B.; Chopra, N.; Rantell, T.; Andrews, R.; Gavalas, V.; Bachas, L. Aligned Multiwalled Carbon Nanotube Membranes. *Science* **2004**, *303*, 62–65.
3. Meitl, M. A.; Zhou, Y. X.; Gaur, A.; Jeon, S.; Usrey, M. L.; Strano, M. S.; Rogers, J. A. Solution Casting and Transfer Printing Single-Walled Carbon Nanotube Films. *Nano Lett.* **2004**, *4*, 1643–1647.
4. Artukovic, E.; Kaempgen, M.; Hecht, D. S.; Roth, S.; Grüner, G. Transparent and Flexible Carbon Nanotube Transistors. *Nano Lett.* **2005**, *5*, 757–760.
5. Ahn, J.; Kim, H.; Lee, K.; Jeon, S.; Kang, S.; Sun, Y.; Nuzzo, R.; Rogers, J. Heterogeneous Three-Dimensional Electronics by Use of Printed Semiconductor Nanomaterials. *Science* **2006**, *314*, 1754–1757.
6. Zhang, D. H.; Ryu, K.; Liu, X. L.; Polikarpov, E.; Ly, J.; Tompson, M. E.; Zhou, C. W. Transparent, Conductive, and Flexible Carbon Nanotube Films and Their Application in Organic Light-Emitting Diodes. *Nano Lett.* **2006**, *6*, 1880–1886.
7. Jung, Y. J.; Kar, S.; Talapatra, S.; Soldano, C.; Viswanathan, G.; Li, X. S.; Yao, Z. L.; Ou, F. S.; Avadhanula, A.; Vajtai, R.; *et al.* Aligned Carbon Nanotube–Polymer Hybrid Architectures for Diverse Flexible Electronic Applications. *Nano Lett.* **2006**, *6*, 413–418.
8. Kang, S.; Kocabas, C.; Ozel, T.; Shim, M.; Pimparkar, N.; Alam, M.; Rotkin, S.; Rogers, J. High-Performance Electronics Using Dense, Perfectly Aligned Arrays of Single-Walled Carbon Nanotubes. *Nat. Nanotechnol.* **2007**, *2*, 230–236.
9. Cao, Q.; Rogers, J. A. Ultrathin Films of Single-Walled Carbon Nanotubes for Electronics and Sensors: A Review of Fundamental and Applied Aspects. *Adv. Mater.* **2009**, *21*, 29–53.
10. Snow, E.; Perkins, F.; Houser, E.; Badescu, S.; Reinecke, T. Chemical Detection with a Single-Walled Carbon Nanotube Capacitor. *Science* **2005**, *307*, 1942–1945.
11. Li, W.; Xie, S.; Qian, L.; Chang, B.; Zou, B.; Zhou, W.; Zhao, R.; Wang, G. Large-Scale Synthesis of Aligned Carbon Nanotubes. *Science* **1996**, *274*, 1701–1703.
12. Fan, S. S.; Chapline, M. G.; Franklin, N. R.; Tombler, T. W.; Cassell, A. M.; Dai, H. J. Self-Oriented Regular Arrays of Carbon Nanotubes and Their Field Emission Properties. *Science* **1999**, *283*, 512–514.
13. Wei, B. Q.; Vajtai, R.; Jung, Y.; Ward, J.; Zhang, R.; Ramanath, G.; Ajayan, P. M. Organized Assembly of Carbon Nanotubes—Cunning Refinements Help To Customize the Architecture of Nanotube Structures. *Nature* **2002**, *416*, 495–496.
14. Shimoda, H.; Oh, S.; Geng, H.; Walker, R.; Zhang, X.; McNeil, L.; Zhou, O. Self-Assembly of Carbon Nanotubes. *Adv. Mater.* **2002**, *14*, 899–901.
15. Rao, S. G.; Huang, L.; Setyawan, W.; Hong, S. H. Large-Scale Assembly of Carbon Nanotubes. *Nature* **2003**, *425*, 36–37.
16. Xiong, X.; Jaberansari, L.; Hahm, M.; Busnaina, A.; Jung, Y. Building Highly Organized Single-Walled-Carbon-Nanotube Networks Using Template-Guided Fluidic Assembly. *Small* **2007**, *3*, 2006–2010.
17. LeMieux, M.; Roberts, M.; Barman, S.; Jin, Y.; Kim, J.; Bao, Z. Self-Sorted, Aligned Nanotube Networks for Thin-Film Transistors. *Science* **2008**, *321*, 101–104.
18. Jiao, L.; Xian, X.; Wu, Z.; Zhang, J.; Liu, Z. Selective Positioning and Integration of Individual Single-Walled Carbon Nanotubes. *Nano Lett.* **2009**, *9*, 205–209.
19. Barber, A.; Cohen, S.; Wagner, H. Static and Dynamic Wetting Measurements of Single Carbon Nanotubes. *Phys. Rev. Lett.* **2004**, *92*, 186103.
20. Wang, C.; Waje, M.; Wang, X.; Tang, J. M.; Haddon, R. C.; Yan, Y. Proton Exchange Membrane Fuel Cells with Carbon Nanotube Based Electrodes. *Nano Lett.* **2004**, *4*, 345–348.
21. Kordas, K.; Toth, G.; Moilanen, P.; Kumpumaki, M.; Vahakangas, J.; Uusimaki, A.; Vajtai, R.; Ajayan, P. M. Chip Cooling with Integrated Carbon Nanotube Microfin Architectures. *Appl. Phys. Lett.* **2009**, *90*, 123105.
22. Cheng, H. M.; Yang, Q. H.; Liu, C. Hydrogen Storage in Carbon Nanotubes. *Carbon* **2001**, *39*, 1447–1454.
23. Beebe, D. J.; Moore, J. S.; Yu, Q.; Liu, R. H.; Kraft, M. L.; Jo, B. H.; Devadoss, C. Microfluidic Tectonics: A Comprehensive Construction Platform for Microfluidic Systems. *Proc. Natl. Acad. Sci. U.S.A.* **2000**, *97*, 13488–13493.
24. Monahan, J.; Gewirth, A. A.; Nuzzo, R. G. A Method for Filling Complex Polymeric Microfluidic Devices and Arrays. *Anal. Chem.* **2001**, *73*, 3193–3197.
25. Burg, T. P.; Manalis, S. R. Suspended Microchannel Resonators for Biomolecular Detection. *Appl. Phy. Lett.* **2003**, *83*, 2698–2700.
26. Shaikh, K. A.; Ryu, K. S.; Goluch, E. D.; Nam, J. M.; Liu, J.; Thaxton, C. S.; Chiesl, T. N.; Barron, A. E.; Lu, Y.; Mirkin, C. A. A Modular Microfluidic Architecture for Integrated Biochemical Analysis. *Proc. Natl. Acad. Sci. U.S.A.* **2005**, *102*, 9745–9750.
27. Valentini, L.; Cantalini, C.; Armentano, I.; Kenny, J.; Lozzi, L.; Santucci, S. Highly Sensitive and Selective Sensors Based on Carbon Nanotubes Thin Tilms for Molecular Detection. *Diamond Relat. Mater.* **2004**, *13*, 1301–1305.
28. Sin, M. L. Y.; Chow, G. C. T.; Wong, G. M.; Li, K. W. J.; Leong, P. H. W.; Wong, K. W. Ultralow-Power Alcohol Vapor Sensors Using Chemically Functionalized Multiwalled Carbon Nanotubes. *IEEE Trans. Nanotechnol.* **2007**, *6*, 571–577.
29. Jaber-Ansari, L.; Hahm, M.; Somu, S.; Sanz, Y.; Busnaina, A.; Jung, Y. Mechanism of Very Large Scale Assembly of SWNTs in Template Guided Fluidic Assembly Process. *J. Am. Chem. Soc.* **2008**, *131*, 804–808.
30. Hahm, M. G.; Kwon, Y.-K.; Lee, E.; Ahn, C. W.; Jung, Y. J. Diameter Selective Growth of Vertically Aligned Single Walled Carbon Nanotubes and Study on Their Growth Mechanism. *J. Phys. Chem. C* **2008**, *112*, 17143–17147.
31. Takagi, D.; Homma, Y.; Hibino, H.; Suzuki, S.; Kobayashi, Y. Single-Walled Carbon Nanotube Growth from Highly Activated Metal Nanoparticles. *Nano Lett.* **2006**, *6*, 2642–2645.